Available online at www.sciencedirect.com
ScienceDirect
Planetary and Space Science 56 (2008) 1542–1551
Planetary and Space Science
www.elsevier.com/locate/pss

Numerical simulation of small-scale low-β magnetic flux ropes in the upper ionospheres of Venus and Mars

Hironori Shimazu[a,b,c,*], Motohiko Tanaka[d]

[a]*Applied Electromagnetic Research Center, National Institute of Information and Communications Technology, Koganei, Tokyo 184-8795, Japan*
[b]*Space Environment Research Center, Kyushu University, Fukuoka, Japan*
[c]*CREST, JST, Japan*
[d]*Coordination Research Center, National Institute for Fusion Science, 322-6 Oroshi-cho, Toki 509-5292, Japan*

Received 18 May 2007; received in revised form 31 May 2008; accepted 7 July 2008
Available online 24 July 2008

Abstract

We use a three-dimensional macro-particle code (implicit-particle simulation) to examine the evolution of a small magnetic flux rope, where "small" means that its radius is close to the kinetic length scale of protons or electrons. Small flux ropes have been observed in the dayside ionospheres of Venus and Mars. In our simulations, we assume that the initial low-β force-free flux rope is maintained by the electron current: an electron beam flows in the flux rope along the magnetic field lines. The simulation results show that electrostatic two-stream (Buneman) instability is generated around the flux rope axis where the velocity of the electron beam is higher than the electron thermal velocity or the acoustic velocity. Electrons there are heated considerably in the direction parallel to the magnetic field by the instability, and an electron hot tube is formed. The magnetic field deviates from the initial force-free field although the helical structure of the magnetic field is maintained. These results indicate that the electron hot tubes will be evidence of flux rope formation in the low-β region, i.e., in the interaction region between the solar wind and the ionosphere, if they are found by high-resolution observations in the upper ionosphere.

Keywords: Magnetic flux rope; Venus; Mars; Two-stream instability

1. Introduction

Magnetic flux ropes have been observed over a wide range of parameter regimes in interplanetary space (Burlaga et al., 1981), at the magnetopause of the earth as a flux transfer event (Elphic, 1990), in the geomagnetic tail (Sibeck, 1990), and in the active regions of the solar photosphere (Parker, 1979). In a flux rope, the plasma β value (ratio of plasma thermal energy to magnetic energy) is generally low, and the magnetic field is almost force-free, as shown by in situ interplanetary space observations (Burlaga, 1988). Such force-free flux ropes are stable in the magnetohydrodynamics (MHD) regime when the pressure is uniform. They are the final state of magnetic field relaxation, conserving the magnetic helicity when there is small dissipation (minimum energy principle) (Taylor, 1974; Kusano et al., 1995).

An interesting question is whether the kinetic effects destabilize force-free flux ropes when the flux rope radius is close to the kinetic length scale of protons or electrons. We call such a flux rope a "small flux rope." As far as we know, the kinetic effects on small flux ropes have not been studied. We are interested in whether small flux ropes have the same properties as MHD-scale flux ropes, which are stable when the pressure is uniform.

Small flux ropes have been observed in the ionosphere on the dayside of Venus by the Pioneer Venus Orbiter (PVO) (Russell and Elphic, 1979). Their radius (~10 km) is of the order of the proton cyclotron radius (~3 km) (Elphic and Russell, 1983a). Small flux ropes have also been found in

*Corresponding author at: Applied Electromagnetic Research Center, National Institute of Information and Communications Technology, Koganei, Tokyo 184-8795, Japan. Tel.: +81 42 327 6516; fax: +81 42 327 6661.
E-mail addresses: hironori.shimazu@gmail.com (H. Shimazu), mtanaka@nifs.ac.jp (M. Tanaka).

0032-0633/$ - see front matter © 2008 Elsevier Ltd. All rights reserved.
doi:10.1016/j.pss.2008.07.007

the ionosphere of Mars by the Mars Global Surveyor (Cloutier et al., 1999; Vignes et al., 2004).

A possible mechanism for the generation of small flux ropes in the Venus ionosphere is Kelvin–Helmholtz instability at the boundary between the ionospheric and solar wind plasmas (Wolff et al., 1980). Luhmann and Elphic (1985) suggested that they are the result of a kinematic dynamo process acting on weak seed fields in the ionosphere. Kleeorin et al. (1994) postulated that they are due to amplification of the magnetic fluctuations in the ionosphere by dynamo action. Cole (1994) argued that the solar wind dynamo action was a mechanism at high altitudes. Generally, the flux rope formation locations have been considered to be the ionosphere itself or the ionosphere–solar wind interaction region.

One of the noticeable differences between the two regions is plasma β values. In the upper atmosphere of Venus or Mars, the magnetic barrier (ionosphere–solar wind interaction region) is characterized by low-β plasmas (Zhang et al., 1991). On the other hand, in the ionosphere, β is high. In this paper, we assume that the plasma β is low when flux ropes are generated. We examine how they develop under this assumption and aim to impose restrictions on the locations where the flux ropes form.

A small flux rope requires a large electric current to maintain its magnetic field. Therefore, considering small flux ropes is equivalent to considering strong flux ropes. If the velocity of electrons carrying the current is larger than some threshold, two-stream instability can be generated. This possibility was suggested by Elphic and Russell (1983a). However, detailed research about it has not been conducted so far.

Using numerical simulations, we investigate the evolution of small flux ropes after formation. In Section 2, we describe our simulation methods. Before showing the simulation results, we estimate the instability criterion for the flux rope radius and the β value in Section 3. The simulation results are presented in Section 4. We find that electrons are heated considerably by the two-stream instability. The applications of our findings to the Venus ionosphere and our estimate of the heating rate are described in Section 5.

2. Methods

We use the three-dimensional macro-particle code (implicit-particle code) described by Tanaka (1988) to investigate the evolution of small-scale flux ropes. The code has been tested and proved valid under various conditions, including Alfvén ion-cyclotron instability (Tanaka, 1993), collisionless magnetic reconnection (Tanaka, 1995), and collisionless shocks (Shimazu et al., 1996). In this code, ions are treated as macro-particles with full kinetic motion. Drift kinetic equations with a guiding center approximation for perpendicular motion are used for electrons; the inertia term is retained for motion along the magnetic field, and the magnetic moment of each electron is assumed to be conserved. The reason for using the guiding center approximation is that the electric field generated by electrostatic two-stream (Buneman) instability considered in this paper is almost parallel to the magnetic field in the linear phase. We examined several cases that include the electron cyclotron motion. The results do not exhibit any clear difference from those for the guiding center approximation.

To retain only low-frequency (large spatial scale) phenomena, a slightly backward time-decentered scheme is used in the Maxwell equations and the equations of motion. The slightly backward time-decentered scheme means that we take $\alpha = 0.6$ in a discrete form,

$$x^{n+1} - x^n = \Delta t f^{n+\alpha} \tag{1}$$

for a differential equation

$$\frac{\mathrm{d}x}{\mathrm{d}t} = f. \tag{2}$$

The value $\alpha = 0.6$ allows us to make calculation with good accuracy and without the constraint of the Courant–Friedrichs–Lewy condition. The code treats three spatial dimensions, three components of particle velocities, and all three components of the electric and magnetic fields. We do not introduce phenomenological resistivity (friction) in the equations.

The simulations are performed as an initial and boundary value problem. We solve the equations in Cartesian coordinates (x, y, and z). The initial cylindrical flux rope has its symmetry axis parallel to the z-axis. The simulation box is a cubic box of size $x_{\max} = y_{\max} = z_{\max} = 50c/\omega_{\mathrm{pe}}$, where $\omega_{\mathrm{pe}} = (4\pi n_0 e^2/m_{\mathrm{e}})^{1/2}$ is the electron plasma frequency, e is the unit charge, m_{e} is the electron mass, n_0 is the number density of the plasma, and c is the speed of light. The number of grid points is 64 in each of the x, y, and z directions.

As an initial condition, we assume that the flux rope is maintained only by the electron current. This assumption is reasonable because the proton current alone cannot make a structure smaller than the proton cyclotron radius. Protons are assumed to have no bulk drift except for thermal motion. The initial electron bulk velocity is given by

$$v_{\mathrm{e}z} = -\frac{cB_0}{2\pi e n_0 r_0 (1 + r^2/r_0^2)^2}, \tag{3}$$

$$v_{\mathrm{e}\theta} = \frac{r v_{\mathrm{e}z}}{r_0}, \tag{4}$$

where $v_{\mathrm{e}z}$ and $v_{\mathrm{e}\theta}$ are the axial and azimuthal components of the electron bulk velocity, respectively, r_0 is a measure of the flux rope radius, $B_0 = 1.0 \times 10^{-3} m_{\mathrm{e}} c \omega_{\mathrm{pe}}/e$ is a constant representing the magnetic field strength along the flux rope axis, and r is the radial distance from the axis.

We use the axisymmetric force-free magnetic field proposed by Gold and Hoyle (1960):

$$B_z = \frac{B_0}{1 + r^2/r_0^2}, \tag{5}$$

$$B_\theta = \frac{rB_z}{r_0}, \tag{6}$$

where B_z and B_θ are the axial and azimuthal components of the magnetic field, respectively. The assumption of a force-free field is good for flux ropes observed in the ionosphere of Venus, as shown by Ledvina et al. (2002).

Note that the initial magnetic field is generated by electric current flowing in the simulation box: $\boldsymbol{J}_e = -en_0(v_{ez}\hat{\boldsymbol{z}} + v_{e\theta}\hat{\boldsymbol{\theta}})$, where $\hat{\boldsymbol{z}}$ and $\hat{\boldsymbol{\theta}}$ are the unit vectors in the axial and azimuthal directions, respectively. In the initial equilibrium, the electrons move along the magnetic field lines, and this electric current generates the magnetic field of the flux rope given by Eqs. (5) and (6).

The simulated plasmas consist of protons and electrons, and the mass ratio m_i/m_e is 100, where m_i is the proton mass. The maximum growth rate of the Buneman instability considered in this paper depends weakly on the mass ratio (proportional to the $\frac{1}{6}$th power of the mass ratio) (Gary, 1993). Thus, the artificial mass ratio has little influence on the time scale, at least in the linear phase.

Timestep Δt is $100\omega_{pe}^{-1}$ ($= 10\omega_{pi}^{-1}$, where ω_{pi} is the proton plasma frequency). The validity of this timestep in this implicit code has been verified by test particle tracking and the solution of the dispersion relation, as shown later in this paper. The plasma density n_0 and pressure are initially uniform. Since the magnetic field is force-free, pressure equilibrium is naturally achieved. A periodic boundary condition is applied in the z direction, and a particle reflection boundary condition is applied in the x and y directions.

3. Analysis

As is well known, the fastest growing two-stream instability is the Buneman instability, when both protons and electrons are cold (Shimada and Hoshino, 2003). When protons and electrons are not cold, either the electrostatic ion-cyclotron or ion-acoustic wave instability can grow. The linear theory shows that the growth rate of the electrostatic ion-cyclotron wave instability is larger than that of the ion-acoustic wave instability when the temperature of protons is the same as that of electrons (Kindel and Kennel, 1971).

When the beam velocity is close to the electron drift velocity, a modified two-stream instability can also be generated (Tanaka and Papadopoulos, 1983). The generated wave is the lower hybrid wave. It is an electrostatic wave that propagates almost perpendicularly to the magnetic field. As shown later in this paper, the simulation results do not show waves propagating perpendicularly to the magnetic field. Therefore, we do not consider modified two-stream instability. The current flowing along the magnetic field can also lead to a kink-type instability as well. The growth rates of the kink instability and the internal kink instability are generally much smaller than that of the Buneman instability. Here, the kink-type instability is not effective.

Roughly speaking, these instabilities can be excited when the drift velocity u exceeds the electron thermal velocity $v_{e,th}$ or the acoustic velocity. Here, we consider the relation between u and $v_{e,th}$ as a guideline and estimate the instability criterion. If we substitute u as v_{ez} at $r = 0$ in Eq. (3), $u > v_{e,th}$ yields

$$r_0 < \frac{c}{\omega_{pe}}\frac{2}{\sqrt{\beta}}. \tag{7}$$

Therefore, when the plasma β value is close to unity, flux ropes whose radius is smaller than the electron inertial length are unstable in the two-stream instability. When β is less than unity, flux ropes whose radius is larger than the electron inertial length can be unstable in the two-stream instability.

It has been widely accepted that the magnetic field in the flux rope can be approximated by the force-free field (Ledvina et al., 2002). This means that β is very low when it is formed. If β is high, the effect of plasma pressure prevails over that of the magnetic pressure. The structure originating in the magnetic field is not easily excited in high-β plasmas. For interplanetary flux ropes, β is 10^{-1}–10^{-2} at the corona when they are formed (Parker, 1979).

We assume from the above discussion that β is low at the location where the flux rope is generated. In this paper, the initial β values for both protons and electrons are assumed to be 0.01. Thus, we are considering flux rope formation in or around the magnetic barrier region (ionosphere–solar wind interaction region). By contrast, the observations in the ionospheric flux ropes showed that β values at the peak magnetic field range from 1 to 3 (Elphic and Russell, 1983a), which is higher than that in the magnetic barrier, but lower than that of the surrounding plasmas in the ionosphere. In this paper, we will show that the β value in the flux ropes can increase by more than 10 times because of heating due to the instability. Considering the interaction with the surrounding high-β plasmas after they are transported into the ionosphere, β values in the flux ropes may be of the order of unity in the ionosphere, even if they start with $\beta = 0.01$. The relatively low-β values in the ionospheric flux ropes compared with the surrounding plasmas may be a remnant of the formation in the low-β region. In any case, this study is not applicable to flux rope formation in the lower ionosphere (high-β region).

When we use this β value, $v_{e,th}$ becomes $1.0 \times 10^{-4}c$. We consider here the case of $u = 2v_{e,th}$, because the maximum $u/v_{e,th}$ in the flux ropes was 1.88, as observed in the Venus ionosphere (Elphic and Russell, 1983a). There are some possibilities that the resolution of the PVO observations was not always sufficient to estimate the electron velocity in the flux rope. However, many flux ropes have been reported based on the PVO observations. Here we refer to the PVO results.

In this case, the proton cyclotron radius u/(cyclotron frequency) is $2c/\omega_{pe}$, and $r_0 = 10c/\omega_{pe}$. The electron

inertial length c/ω_{pe} is of the order of tens of meters for typical electron densities of $10^4-10^5\,cm^{-3}$ in the Venus ionosphere, and the proton inertial length c/ω_{pi} ranges from several hundred meters to several kilometers.

4. Simulation results

4.1. Linear phase

Fig. 1 shows the development of the electric field parallel to the magnetic field and the phase space densities of protons and electrons along the flux rope axis (for $r<0.5r_0$). Wave excitation in the parallel electric field is evident at $\omega_{pi}t = 4400$. Electrons and protons are trapped in the parallel direction by the waves. Fig. 1c shows that the electrons are heated considerably in the direction parallel to the magnetic field in the late phase at $\omega_{pi}t = 6800$, while ions are not much affected by the instability.

The predominant wavelength observed in the simulation is $\lambda_{\parallel} \cong 1c/\omega_{pe}$ in the direction parallel to the magnetic field. The wave number perpendicular to the magnetic field is not observed. The electron temperature in the perpendicular direction does not change, as shown in Fig. 1. Therefore, electrostatic ion-cyclotron wave instability and modified two-stream instability are not responsible for the observed process. We solve the dispersion relation of Buneman instability for a uniform plasma and magnetic

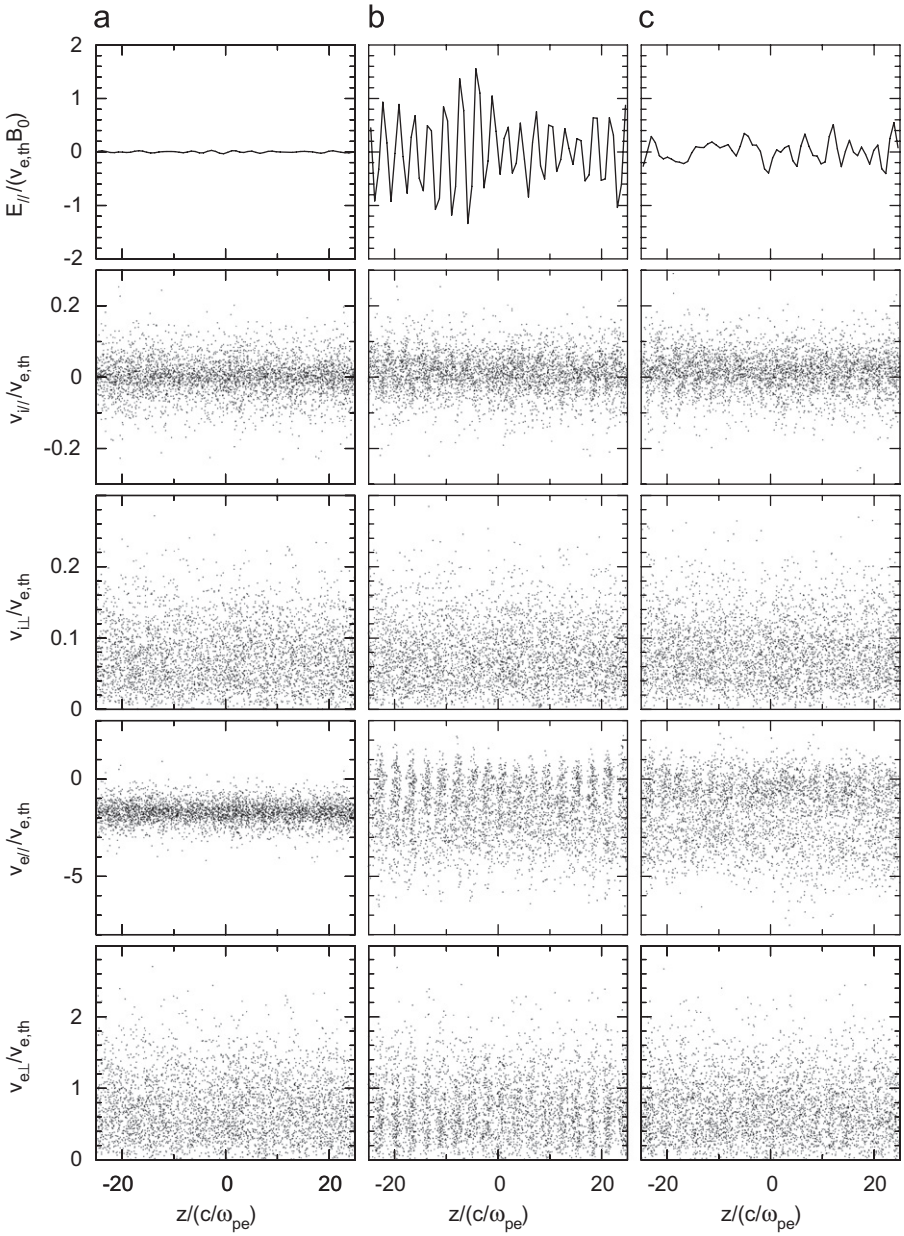

Fig. 1. Quantity along the flux rope axis ($x = y = 0$ line): (from the top) electric field component parallel to the magnetic field ($E_{\parallel}$), proton velocity parallel to the magnetic field ($v_{i\parallel}$), proton velocity perpendicular to the magnetic field ($v_{i\perp}$), electron velocity parallel to the magnetic field ($v_{e\parallel}$), and electron velocity perpendicular to the magnetic field ($v_{e\perp}$) at $\omega_{pi}t =$ (a) 200, (b) 4400, and (c) 6800.

field, which should be applicable to the region around the flux rope axis, and obtain

$$1-\frac{\omega_{\mathrm{pe}}^2}{(\omega-ku)^2}-\frac{\omega_{\mathrm{p}i}^2}{\omega^2}=0, \tag{8}$$

where ω is the angular frequency and k is the wave number. The solution to Eq. (8) shows that the growth rate γ is approximately $0.00198\omega_{\mathrm{p}i}$ $(2\pi/\gamma=3170\omega_{\mathrm{p}i}^{-1})$ for wavelength $\lambda_{\parallel}\cong 1c/\omega_{\mathrm{pe}}$. The growth rate is slow in this case, because u is not so large for the waves to grow fast. Thus, Buneman instability accounts well for the observed wave growth.

The results of our simulation show that the growth rate of the Buneman instability is independent of the curvature of the magnetic field, as long as the length scale of the curvature is larger than or close to the ion-cyclotron radius. Since the time scale of the growth is much shorter than the ion-cyclotron period, curvature does not affect the ion motion. For electrons, the length scale of the curvature of the magnetic field lines is much larger than their cyclotron radius. Moreover, the electron beam velocity is low in the edge region (apart from the axis), where the curvature is effective. Thus, the effect of the magnetic field and the curvature is small in the Buneman instability.

Electric currents along and transverse to the magnetic field lines are not independent, in particular if the curvature of the magnetic field lines approaches the flux rope radius. In our simulation, however, the time scale of the growth is much shorter than the ion-cyclotron period. Moreover, the

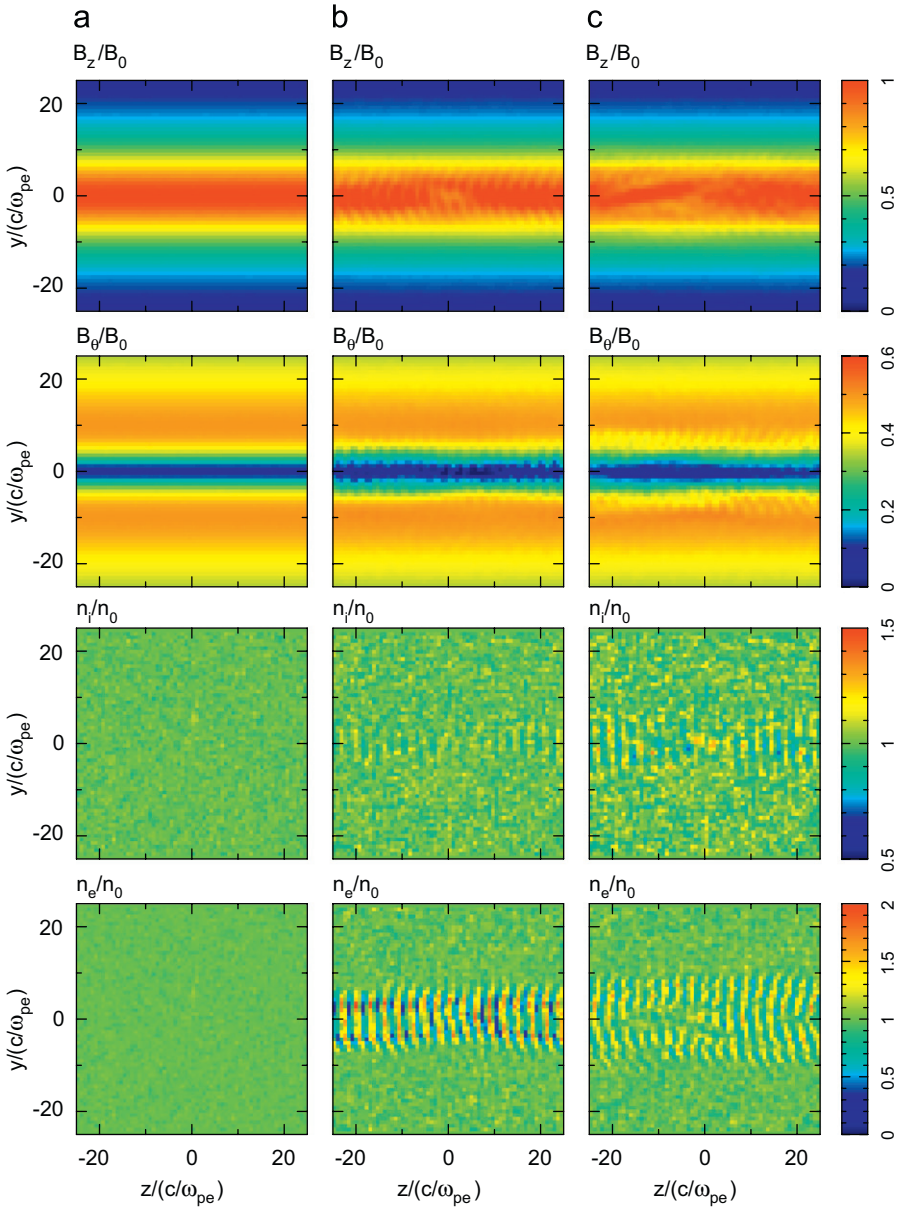

Fig. 2. Quantity on the $x=0$ plane (plane including the flux rope axis): (from the top) axial component of the magnetic field (B_z), azimuthal component of the magnetic field (B_θ), proton density (n_i), and electron density (n_e) at $\omega_{\mathrm{p}i}t=$ (a) 200, (b) 4400, and (c) 6800.

length scale of the curvature of the magnetic field lines is much larger than the cyclotron radius of electrons carrying the current. Thus, the electron bulk motion generating the current is regarded to be parallel to the magnetic field at least initially. In the simulation, we have measured the perpendicular motion of each electron. The results show that the electrons have no perpendicular bulk motion even after the saturation (the third panels from the above in Fig. 1). The perpendicular velocity component does not affect the instability, even if the magnetic field line curvature is close to the flux rope radius.

The magnetic field and plasma densities of protons and electrons on the $x=0$ plane (plane including the flux rope axis) are shown in Fig. 2. A fishbone-like wave structure along the axis is evident in the electron density at $\omega_{pi}t=4400$ in the center of the panel. Buneman instability grows more rapidly near the axis because the electron velocity is higher closer to the axis. The wave pattern appears to move in the negative z direction because the electrons have a bulk velocity in the negative z direction. Since the electrons move faster to the negative z direction at the rope axis than in the surrounding region, the pattern in the figure changes from a straight stripe to a curved one over time, as shown in Figs. 2b and c. A sawtooth pattern in the magnetic field is also observed in Figs. 2b and c; it is caused by the current decrease due to the instability.

Fig. 3 shows the magnetic field and plasma density at $\omega_{pi}t=4400$ on the $z=0$ plane (plane perpendicular to the flux rope axis, which is at the center of each panel). A marked vortex structure in electron density, which marks the nonlinear stage, is evident around the center, while no significant changes appear in the proton density. The low-density (rarefaction) and the high-density (condensation) phases that are generated by the instability are aligned along the magnetic field lines that penetrate this vortex. As a result, the vortex structure appears in the electron density on the plane perpendicular to the rope axis.

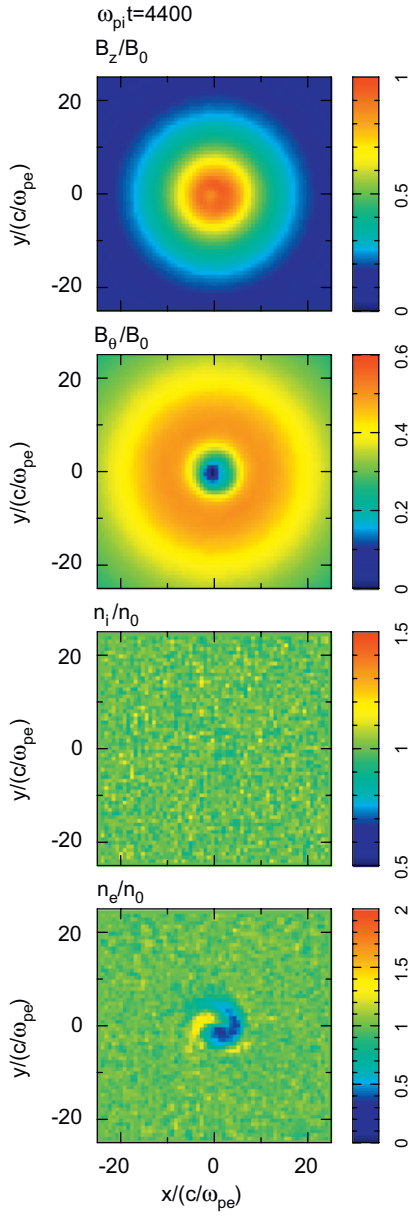

Fig. 3. Quantity on the $z=0$ plane (plane perpendicular to the flux rope axis, which is at the center of each panel): (from the top) axial component of the magnetic field (B_z), azimuthal component of the magnetic field (B_θ), proton density (n_i), and electron density (n_e) at $\omega_{pi}t=4400$.

4.2. Nonlinear phase

The time history of the electron temperature T parallel to the magnetic field in the flux rope is shown in Fig. 4. Between $\omega_{pi}t=3000$ and 5000, the temperature increases sharply. The temperature is four times the initial one in the flux rope $r<r_0$. If we consider only the region near the axis ($r<0.5r_0$), the temperature is 10 times the initial one. Strong heating occurs near the flux rope axis. The electron distribution functions parallel to the magnetic field for the region $r<r_0$ are shown in Fig. 5. At $\omega_{pi}t=200$, the peak is located at around $v_{e\parallel}/v_{e,th}\cong -2$. As time passes, the distribution spreads. When the distribution function shifts

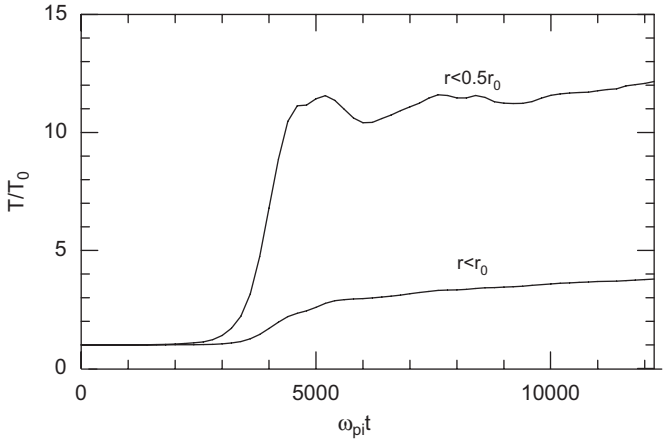

Fig. 4. Time history of electron temperature T parallel to the magnetic field in regions $r<r_0$ and $r<0.5r_0$. T_0 represents the initial temperature $m_e v_{e,th}^2/2$.

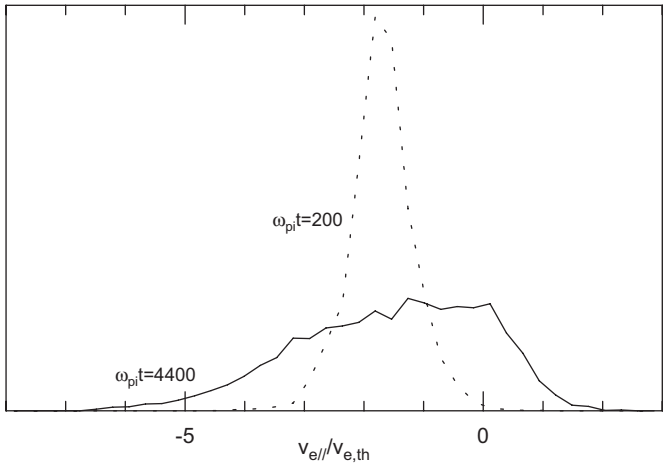

Fig. 5. Distribution functions of the electron velocity parallel to the magnetic field in the region $r<r_0$ at $\omega_{pi}t=200$ and 4400. The values on the vertical axis are normalized by the peak value of the distribution function at $\omega_{pi}t=200$.

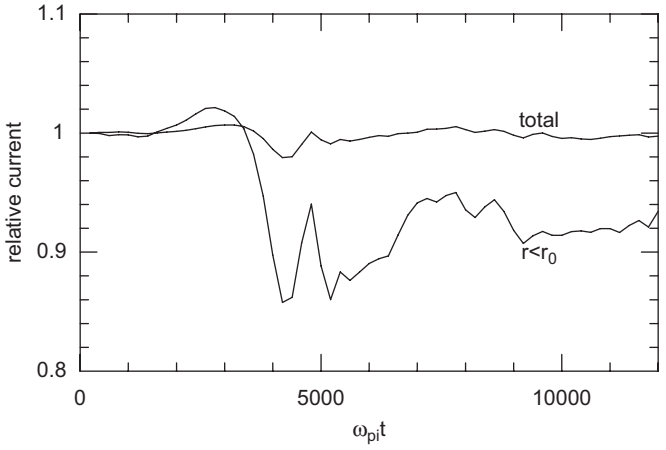

Fig. 6. Time history of the electric current carried by electrons crossing the $z=0$ plane (total and the $r<r_0$ region). Each initial current was normalized to 1.

toward $v_{e\parallel}=0$ and becomes almost flat at $\omega_{pi}t=4400$, the instability saturates.

In the lower ionosphere of Venus, the time scale for the temperature increase is comparable with the electron–neutral collision time. As stated earlier in this paper, however, we consider the flux rope generation that occurs in the upper ionosphere or in the interaction region between the solar wind and the ionosphere. The time scale for the temperature increase is much shorter than the electron–neutral collision time there, and it is not necessary to consider the electron–neutral collision here.

The time development of the electric current carried by electrons crossing the $z=0$ plane (plane perpendicular to the flux rope axis) is shown in Fig. 6. Positive ions do not carry the current during the simulation run. The electron current in the region $r<r_0$ decreases by approximately 10% as the instability proceeds. By contrast, the total electric current crossing the whole $z=0$ plane is mostly conserved. This indicates that the current in the flux rope scatters in the radial directions to the outside of the rope because of the strong heating near the rope axis.

Although the helical structure of the magnetic field lines is maintained after the saturation of the instability, the magnetic field deviates from the initial force-free field. The spatial profile of the magnetic field in the flux rope is shown in Fig. 7. A notable feature is the decrease in B_θ and B_z around the rope axis at $\omega_{pi}t=4400$. Combined with the result from Fig. 6, the decrease of B_θ and B_z around the axis corresponds to the current decrease in the flux rope due to the instability and the outward scattering of the current.

The spatial profiles of T and electron drift velocity u at $\omega_{pi}t=6800$ are shown in Fig. 8. We find that the volume where T is very high is localized only near the flux rope axis ($r=0$), where the instability occurred. We call this high-temperature region around the flux rope axis *an electron hot tube*.

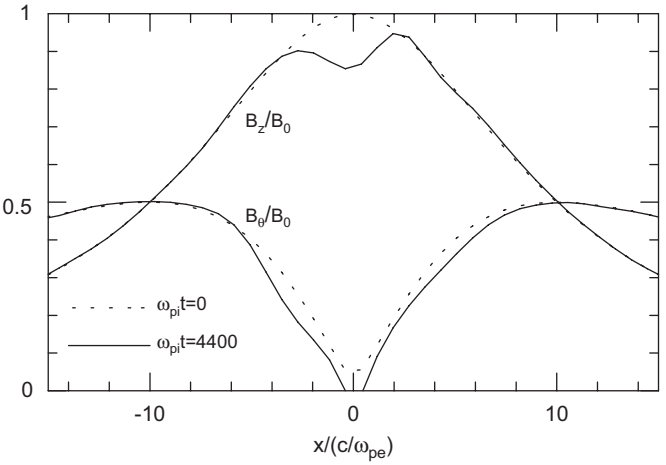

Fig. 7. Spatial profile of the magnetic field along the $y=z=0$ line (perpendicular to the flux rope axis).

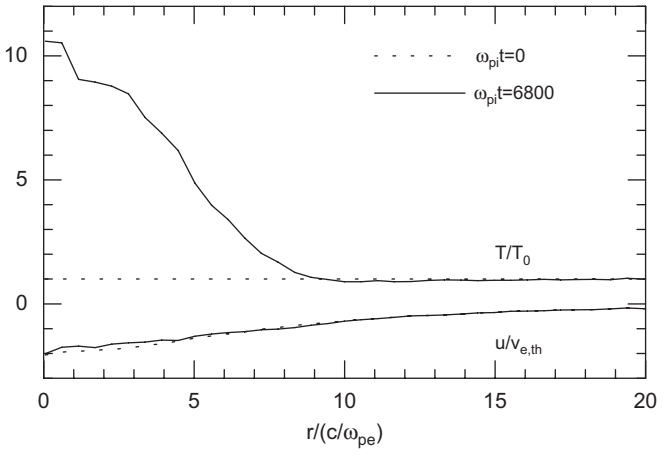

Fig. 8. Spatial profiles of the temperature T and electron drift velocity u averaged over the azimuthal direction.

If a small-scale flux rope in which the ratio of the electron beam velocity to the electron thermal velocity is larger than unity is generated, the ratio will become less than unity rapidly as a result of the Buneman instability. As a result, only the flux ropes with the ratio less than unity could be observed. If the electron hot tubes are found near the axis of the flux rope with high-resolution observations, the ratio may be larger than unity when it is generated. The high-resolution observation may give us a clue to the flux rope generation process.

The simulation results show that the total electron kinetic energy in the entire simulation box is conserved to within 2% from $t=0$ to $\omega_{pi}t=10,000$. The energy may not be conserved in the real flux ropes at Venus or Mars, since the magnetic field lines in the top-side ionosphere may be connected with the interplanetary magnetic field lines. Electrons can move fast to interplanetary space along the magnetic field lines. When we apply our results to the real Venus flux ropes, we must note this fact.

The equilibrium in the flux rope changes because of the generation of the electron hot tube. Initially, the magnetic field is force-free, and the temperature and density are uniform. After the instability saturates, the structure shown in Figs. 7 and 8 is maintained. As shown in Fig. 7, B_z decreases more than B_θ does at the flux rope axis after the saturation. The B_θ component, whose ratio to B_z increases, causes the Lorentz force in the radially inward direction. The results show that the force balances the pressure gradient force caused by the high temperature around the axis.

The instability does not lead to flux ropes collapse. We had expected that the flux rope would collapse before we carried out these simulations. However, the electric currents in space cannot be turned off easily. The small-scale flux ropes survive for a long time after the electrons are heated. The helical structure of the magnetic field lines is maintained, although the magnetic field deviates from the force-free state. Belova and Zelenyi (1990) showed that small-scale magnetic perturbations are unlikely unstable in the Venus ionosphere. Our results are in agreement with them in that the small-scale helical structure of the magnetic field lines is maintained.

These features are not caused by numerical errors in electron tracking under conditions of curved magnetic field lines and large velocities parallel to the magnetic field. To verify that particles do not escape from a flux rope with a temporarily fixed magnetic field, we have traced the orbits of test electrons in the field of a small flux rope (Eqs. (5) and (6)) with the same timestep considered above. We find that the plasma density in the flux rope remains constant, which verifies the use of our timestep.

We also examine MHD-scale flux ropes whose radius is much larger than the proton cyclotron radius ($x_{max}=y_{max}=z_{max}=500c/\omega_{pe}$, and $r_0=100c/\omega_{pe}$). In this case, the drift speed is very low, $u \ll v_{e,th}$, and instability does not occur. The density and the magnetic field structure around the flux rope axis do not change. Therefore, the features shown above are characteristic of small flux ropes.

5. Application to Venus ionosphere

We estimate how this heating process affects the Venus ionosphere. As shown in Fig. 4, the final temperature is $T=4T_0$ for $r<r_0$. Thus, the temperature becomes 12,000 K after the instability if the initial temperature is 3000 K, which is a typical value for the Venus ionosphere at an altitude of 300 km. The generated heat Q_1 per volume in a flux rope, assuming an ideal gas, is given by

$$Q_1=\tfrac{3}{2}n_0k_B\Delta T, \tag{9}$$

where k_B is the Boltzmann constant and ΔT is the temperature increase. For $n_0=10^4\,cm^{-3}$ (typical value for the Venus ionosphere at an altitude of 300 km), we get $Q_1=1.9\times10^{-9}\,J\,m^{-3}$. If we use typical values in the magnetic barrier around Venus, Q_1 becomes lower because n_0 in the magnetic barrier is much lower than that in the ionosphere. As shown in the following paragraphs, this value is low compared with the solar EUV (extreme ultraviolet) heating, even if we assume flux rope formation in the ionosphere.

The importance of this heating mechanism in the Venus ionosphere depends on the frequency of flux rope formation and the total volume that flux ropes occupy in the ionosphere. Elphic and Russell (1983b) showed that the occurrence probability of flux ropes at altitudes higher than 300 km is 10–20% and reaches more than 50% at altitudes between 170 and 200 km in the near-subsolar region. If we assume that the flux ropes occupy 10–60% of the Venus ionosphere in space and time, the average heat produced by flux ropes Q_2 ranges from 1.9×10^{-10} to $1.1\times10^{-9}\,J\,m^{-3}$.

We compare the heating produced by flux ropes with the solar EUV heating. The solar EUV flux is the main heat source of electrons in the Venus ionosphere. Although the heating mechanism is totally different between the two, we compare them to determine how much the instability contributes to the total heating. The electron heating rate due to the solar EUV flux is $\sim10^{-8}\,J\,m^{-3}\,s^{-1}$ at the peak altitude ($\sim$140 km) and a solar zenith angle of 0°; it is $\sim10^{-10}\,J\,m^{-3}\,s^{-1}$ at altitudes higher than 300 km and in the terminator region (Cravens et al., 1980).

If we consider the lifetime of flux ropes (transport time out of the ionosphere, the order of hours) as the time scale of the heating, the average rate of heating produced by flux ropes (Q_2/time-scale) is lower than that of the solar EUV heating. Therefore, the heating due to the instability is not effective for the total and average heating in the ionosphere of Venus.

However, it is possible for electrons to be heated locally by the instability. The instability growth time (and electron heating time) observed in the simulation is approximately $6800/\omega_{pi}$. The actual time for Venus is 0.1–0.2 s, which is shorter than the collisional electron cooling times or heat transport times at altitudes higher than approximately

170 km. Thus, electrons are heated "instantaneously" when the flux rope is formed, and the electron hot tubes can be generated before the electron cooling or heat transport sets in.

Since the sampling time of the electron temperature by PVO is ~2 s, the finer electron temperature structure in flux ropes than the sampling time is still unknown. As shown in Fig. 8, the electron temperature near the rope axis is up to 10 times higher than that outside the rope. The area where the electrons are heated significantly is a few electron inertial lengths wide (approximately 50–200 m). With higher-resolution measurements to resolve such a short length scale, electron hot tubes could be observed near the rope axis in the dayside ionospheres of Venus and Mars.

The cooling time scale is shorter at altitudes lower than approximately 170 km in the Venus ionosphere. Inelastic collision with neutrals causes electron cooling effectively at these altitudes (Shinagawa et al., 1991). Therefore, the electron hot tubes cannot be maintained there. By contrast, if flux ropes are formed at the interaction region between the solar wind and the ionosphere, the electron hot tubes can remain in the upper ionosphere where the cooling time scale is relatively long. Moreover, at higher altitudes, their transport time out of the ionosphere is comparable to the cooling time scale (of the order of hours). Thus, they are maintained at least for that time scale. Since the typical time scale of the diffusion is from 10 min to several hours even in the low-altitude ionosphere (Luhmann et al., 1984; Shinagawa and Cravens, 1988), the magnetic diffusion is negligible, at least at higher altitudes.

Therefore, the existence of the electron hot tube may give us a clue to identify where flux ropes form. If the ropes are formed in a high-β region, the electron hot tubes are not generated. Instead, if the tubes are observed by high-resolution observations in the upper ionosphere, it will be evidence of flux rope formation in the low-β region, i.e., in the interaction region between the solar wind and the ionosphere.

Mahajan et al. (1994) found from PVO observation that the electron temperature is high (6000–10,000 K) near the dayside ionopause. The heat source was considered to be the solar wind. Our simulation results show that small flux ropes can be the source of the local heating. If the ropes are formed near the ionopause, they can heat electrons there. PVO may have observed the temperature averaged over electron hot tubes and other areas. If electron hot tubes are observed near the dayside ionopause by high-resolution measurements, they would be evidence of flux rope formation near the ionopause.

The analysis by Ledvina et al. (2002) showed that flux ropes are force-free at low altitudes and that there is a statistical tendency for thermal pressure variation across ropes at higher altitudes. Our simulation results showed that the thermal pressure variation is generated because of heating due to the instability. Since the profile of the magnetic field deviates from the force-free field at the later stage of the instability, as shown in Fig. 7, our simulation results better describe flux ropes at high altitudes, suggesting that those at high altitudes are affected by the instability.

6. Conclusion

We have shown by simulation that Buneman instability is generated around the axis of small-scale low-β magnetic flux ropes. Since electrons carrying electric current along the magnetic field lines maintain the magnetic field of a flux rope, the electron bulk velocity is set to be large. The drift of electrons relative to that of protons causes Buneman instability when the drift velocity is higher than the thermal velocity. As a result, electrons are heated considerably in the direction parallel to the magnetic field around the rope axis. An electron hot tube is formed there.

This instability reduces the electron current inside the flux rope. However, the instability does not lead to flux ropes collapse. The small-scale flux ropes survive for a long time after the electrons are heated. The helical structure of the magnetic field lines is maintained, although the magnetic field deviates from the initial force-free state.

The results are applied to electron heating in the Venus ionosphere. The heating occurs instantaneously only when flux ropes are formed. The average heating rate of this process is lower than that due to the solar EUV flux.

Our simulation results predict the existence of electron hot tubes in the localized region around the flux rope axis. If electron hot tubes are found in the upper ionospheres of Venus and Mars by high-resolution measurements, they could very likely have been generated in the low-β region, i.e., in the interaction region between the solar wind and the ionosphere.

Acknowledgments

We thank Professor Thomas E. Cravens (University of Kansas) for suggesting that we estimate the heating rate in the Venus ionosphere. We also thank Dr. Hiroyuki Shinagawa, Dr. Naoki Terada, Dr. Masao Nakamura, and Dr. Ken Tsubouchi (National Institute of Information and Communications Technology, Japan) for their stimulating and insightful comments and suggestions during the course of this work. This work was supported by NICT Projects Y223103 and Y202106.

References

Belova, E.V., Zelenyi, L.M., 1990. The model of the velocity shear instabilities at Venusian ionopause and the problem of magnetic flux ropes formation. In: Russell, C.T., Priest, E.R., Lee, L.C. (Eds.), Physics of Magnetic Flux Ropes. Geophysical Monograph Series, vol. 58. AGU, Washington, DC, pp. 433–437.

Burlaga, L., Sittler, E., Mariani, F., Schwenn, R., 1981. Magnetic loop behind an interplanetary shock: Voyager, Helios, and IMP 8 observations. J. Geophys. Res. 86, 6673–6684.

Burlaga, L.F., 1988. Magnetic clouds and force-free fields with constant alpha. J. Geophys. Res. 93, 7217–7224.

Cloutier, P.A., Law, C.C., Crider, D.H., Walker, P.W., Chen, Y., Acuña, M.H., Connerney, J.E.P., Lin, R.P., Anderson, K.A., Mitchell, D.L., Carlson, C.W., McFadden, J., Brain, D.A., Rème, H., Mazelle, C., Sauvaud, J.A., d'Uston, C., Vignes, D., Bauer, S.J., Ness, N.F., 1999. Venus-like interaction of the solar wind with Mars. Geophys. Res. Lett. 26, 2685–2688.

Cole, K.D., 1994. Origin of flux ropes in Venus' ionosphere. J. Geophys. Res. 99, 14951–14958.

Cravens, T.E., Gombosi, T.I., Kozyra, J., Nagy, A.F., Brace, L.H., Knudsen, W.C., 1980. Model calculations of the dayside ionosphere of Venus: energetics. J. Geophys. Res. 85, 7778–7786.

Elphic, R.C., 1990. Observations of flux transfer events: Are FTEs flux ropes, islands, or surface waves? In: Russell, C.T., Priest, E.R., Lee, L.C. (Eds.), Physics of Magnetic Flux Ropes. Geophysical Monograph Series, vol. 58. AGU, Washington, DC, pp. 455–471.

Elphic, R.C., Russell, C.T., 1983a. Magnetic flux ropes in the Venus ionosphere: observations and models. J. Geophys. Res. 88, 58–72.

Elphic, R.C., Russell, C.T., 1983b. Global characteristics of magnetic flux ropes in the Venus ionosphere. J. Geophys. Res. 88, 2993–3003.

Gary, S.P., 1993. Theory of Space Plasma Microinstabilities. Cambridge University Press, Cambridge.

Gold, T., Hoyle, F., 1960. On the origin of solar flares. Mon. Not. R. Astron. Soc. 120, 89–105.

Kindel, J.M., Kennel, C.F., 1971. Topside current instabilities. J. Geophys. Res. 76, 3055–3078.

Kleeorin, N., Rogachevskii, I., Eviatar, A., 1994. A mechanism of magnetic flux rope formation in the ionosphere of Venus. J. Geophys. Res. 99, 6475–6481.

Kusano, K., Suzuki, Y., Nishikawa, K., 1995. A solar flare triggering mechanism based on the Woltjer–Taylor minimum energy principle. Astrophys. J. 441, 942–951.

Ledvina, S.A., Nunes, D.C., Cravens, T.E., Tinker, J.L., 2002. Pressure balance across magnetic flux ropes in the ionosphere of Venus. J. Geophys. Res. 107.

Luhmann, J.G., Elphic, R.C., 1985. On the dynamo generation of flux ropes in the Venus ionosphere. J. Geophys. Res. 90, 12047–12056.

Luhmann, J.G., Russell, C.T., Elphic, R.C., 1984. Time scales for the decay of induced large-scale magnetic fields in the Venus ionosphere. J. Geophys. Res. 89, 362–368.

Mahajan, K.K., Ghosh, S., Paul, R., Hoegy, W.R., 1994. Variability of dayside electron temperature at Venus. Geophys. Res. Lett. 21, 77–80.

Parker, E.N., 1979. Cosmical Magnetic Fields. Oxford University Press, Oxford.

Russell, C.T., Elphic, R.C., 1979. Observation of magnetic flux ropes in the Venus ionosphere. Nature 279, 616–618.

Shimada, N., Hoshino, M., 2003. The dynamics of electron–ion coupling in the shock transition region. Phys. Plasmas 10, 1113–1119.

Shimazu, H., Machida, S., Tanaka, M., 1996. Macroparticle simulation of collisionless parallel shocks generated by solar wind and planetary plasma interactions. J. Geophys. Res. 101, 7647–7658.

Shinagawa, H., Cravens, T.E., 1988. A one-dimensional multispecies magnetohydrodynamic model of the dayside ionosphere of Venus. J. Geophys. Res. 93, 11263–11277.

Shinagawa, H., Kim, J., Nagy, A.F., Cravens, T.E., 1991. A comprehensive magnetohydrodynamic model of the Venus ionosphere. J. Geophys. Res. 96, 11083–11095.

Sibeck, D.G., 1990. Evidence for flux ropes in the Earth's magnetotail. In: Russell, C.T., Priest, E.R., Lee, L.C. (Eds.), Physics of Magnetic Flux Ropes. Geophysical Monograph Series, vol. 58. AGU, Washington, DC, pp. 637–646.

Tanaka, M., 1988. Macroscale implicit electromagnetic particle simulation of magnetized plasmas. J. Comput. Phys. 79, 209–226.

Tanaka, M., 1993. A simulation of low-frequency electromagnetic phenomena in kinetic plasmas of three dimensions. J. Comput. Phys. 107, 124–145.

Tanaka, M., 1995. Macro-particle simulations of collisionless magnetic reconnection. Phys. Plasmas 2, 2920–2930.

Tanaka, M., Papadopoulos, K., 1983. Creation of high-energy electron tails by means of modified two-stream instability. Phys. Fluids 26, 1697–1699.

Taylor, J.B., 1974. Relaxation of toroidal plasma and generation of reverse magnetic fields. Phys. Rev. Lett. 33, 1139–1141.

Vignes, D., Acuña, M.H., Connerney, J.E.P., Crider, D.H., Rème, H., Mazelle, C., 2004. Magnetic flux ropes in the Martian atmosphere: global characteristics. Space Sci. Rev. 111, 223–231.

Wolff, R.S., Goldstein, B.E., Yeates, C.M., 1980. The onset and development of Kelvin–Helmholtz instability at the Venus ionopause. J. Geophys. Res. 85, 7697–7707.

Zhang, T.L., Luhmann, J.G., Russell, C.T., 1991. The magnetic barrier at Venus. J. Geophys. Res. 96, 11145–11153.